Research Article

Yasuhiro Yamazaki*, Keisuke Yoshida, Kazuhiro Okada, Momoka Arai, Yosuke Nakahara and
Yutaro Ota

Development of a small-punch-fatigue test method to evaluate fatigue strength and fatigue crack propagation

Abstract: Herein, fatigue and crack propagation tests were conducted using the small-punch-fatigue (SPF) test to verify its applicability to assess fatigue strength and fatigue crack propagation behavior. During the SPF test, a fatigue crack first initiated at the specimen center and then propagated in the radial direction. In most cases, three fatigue cracks propagated from the specimen center to the radial direction in point symmetry. X-ray computed tomography revealed that the crack initiated by the SPF test had a quarter ellipse shape. Elastic finite element (FE) analysis was conducted to estimate the stress state and stress intensity factor (SIF) of the specimen, and an approximate equation was obtained as a function of the applied load. The experimental results comprising fatigue lives and crack growth rates obtained *via* the SPF test were compared with the conventional uniaxial test data as functions of the stress amplitude and SIF determined *via* elastic FE analysis, respectively. This comparison showed that the SPF test can be applied to the fatigue test and fatigue crack propagation test.

Keywords: small-punch-fatigue test, fatigue strength, fatigue crack propagation

* **Corresponding author: Yasuhiro Yamazaki,** Graduate School of Engineering, Chiba University, 1-33, Yayoicho, Inage-ku, Chiba-shi, Chiba, 263-8522, Japan, e-mail: Y.yamazaki@chiba-u.jp
Keisuke Yoshida, Kazuhiro Okada, Momoka Arai: Graduate School of Science and Engineering, Chiba University, 1-33, Yayoicho, Inage-ku, Chiba-shi, Chiba, 263-8522, Japan
Yosuke Nakahara: Materials & Structural Engineering Group, Technology Platform Center, Technology & Intelligence Integration, IHI Corporation, 1 Shin-Nakahara-cho, Isogo-ku, Yokohama-shi, Kanagawa, 235-8501, Japan
Yutaro Ota: Propulsion Engineering Group, Rocket Development Department, Aero-Engine, Space & Defense Business Area, IHI Corporation, 229, Mizuho-machi Tonogaya, Nishitama-gun, Tokyo, 190-1297, Japan

1 Introduction

To ensure the safety and reliability of engineering components used in thermal and other power plants, periodic inspections are necessary to assess their damage and degradation. Generally, the damage conditions and the remaining fatigue lives of power plant components have been estimated using experimental methods combined with numerical analysis. For example, Zhu *et al.* proposed a fatigue life prediction method in the structure of a pressure vessel based on the relationship between fatigue-crack size and residual strength, which was established according to the permissible residual strength [1]. Gao *et al.* proposed a neuro-fuzzy-based machine learning method to predict the multiaxial fatigue life of various metallic materials [2].

Experimental damage and degradation evaluation methods are broadly classified into destructive and nondestructive testing [3–7]. Destructive testing involves cutting specimens from a structure and is generally considered more reliable than nondestructive testing methods, such as ultrasonic testing techniques [8,9]. However, when sampling relatively large specimens for conventional uniaxial tests, such as tensile, fatigue, and creep tests, considerable damage to the structure can occur. The small-sample-testing technique is a semi-destructive technique used for damage assessment in periodic inspections. It requires only a small-volume specimen cut from the part of the actual component. The small-sample-testing technique is used for quality inspections of the actual component products.

The small punch (SP) test is a semi-destructive small-sample-testing technique used for evaluating the damage and remaining life of small samples. In this test, a small rigid ball punches a small disk (SD) specimen with a diameter ranging from 3 to 10 mm and a thickness of less than a millimeter. The SP test method has been used in the nuclear field for over 30 years to evaluate the ductile to brittle transition temperature of materials and to estimate

their fracture toughness [10–12]. Recently, an SP creep test has been proposed to assess the creep damage of actual components in thermal power plants [13–16]. For assessment using the SPC test, SD specimens are prepared from a small sample (*e.g.*, 20 mm × 30 mm × 10 mm in size), which is cut from the surface of the actual component in thermal plants; moreover, the SPC test is often conducted under temperature-accelerated conditions.

The small-punch-fatigue (SPF) test has been proposed to evaluate the fatigue strength and crack propagation characteristics [17,18]. It is one of the best methods to estimate the damage and remaining fatigue life of the actual components in power plants. As fatigue cracks usually start on the surface of a component, it is important to evaluate the fatigue damage around the surface of the component. The SPF test requires only a small part around the surface of the component; thus, the damage caused by sampling the specimen can be negligible when applying the SPF test for fatigue damage assessments.

In this study, to confirm the validity of the SPF test, we used the SPF test to evaluate the fatigue lives and crack growth rates and compared the test results with those of conventional uniaxial fatigue (CUF) tests. In the following sections, the tested material and experimental procedures are first described. Subsequently, the experimental and analysis results regarding the fatigue crack initiation and propagation morphologies, evaluation of fatigue strength, and evaluation of crack propagation rates are presented and discussed. Finally, the conclusion of this study is presented.

2 Experimental procedures

The polycrystalline Ni-based superalloy IN 718 was used in this study. Tables 1 and 2 list the chemical composition and tensile properties of the tested material. The microstructure of the tested material is shown in Figure 1. The average grain size was approximately 15.9 μm. The SD

Table 1: Chemical composition and heat treatment conditions of the tested material (in wt%)

Fe	Cr	Ni	Mo	Al	Ti	Cu
17.50	17.89	53.93	2.96	0.55	0.98	0.07

Co	Ta	B	C	Mn	Si	P
0.25	0.01	0.0038	0.04	0.09	0.06	0.010

Solution annealing: 1 h at 955°C → water quenching.
Aging: 8 h at 718°C → furnace cool + 8 h at 621°C → air cool.

Table 2: Tensile properties of the tested material

Young's modulus	204 GPa
0.2% proof stress	1,207 MPa
Tensile strength	1,420 MPa
Elongation	21.0%
Reduction of area	39.0%

specimens were machined from a round bar of the alloy. The surface of the SD specimen was polished to mirror smoothness using diamond pastes and choroidal silica before the SPF test. The diameter and thickness of the polished disk specimen were 15 mm and 0.290 ± 0.05 mm, respectively. The thickness of each SD specimen was measured before the SPF test.

Figure 2 schematically illustrates the setup of an SD specimen and the testing jig. The SD specimen was securely fixed between the upper and lower holders made of SUS304 austenitic stainless steel. Cyclic bending load was applied to the specimen using a 5 mm diameter SiC ball. SPF tests were conducted at room temperature at a load ratio R = 0.1 and frequency f = 50 Hz using a sinusoidal waveform on an electrodynamic fatigue testing machine (Asahi seisakusho, FRDS-20). During the SPF test, the surface of the SD specimen was observed, and its movies were recorded using a digital microscope equipped with a video recording device, as shown in Figure 2. In the fatigue tests, the fatigue life was determined by counting the number of cycles until a surface fatigue crack with a length of 300 μm, which is almost comparable with the specimen thickness, was observed on the surface of the SD specimen. In the fatigue crack growth tests, the crack growth rates were measured for the fatigue crack ranging from ~0.3 to 1.5 mm in length measured on the specimen surface (given in detail in Section 3.3).
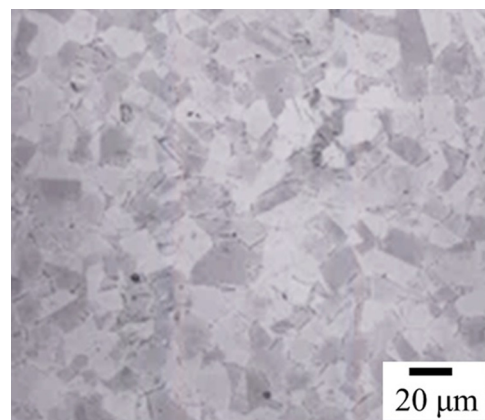

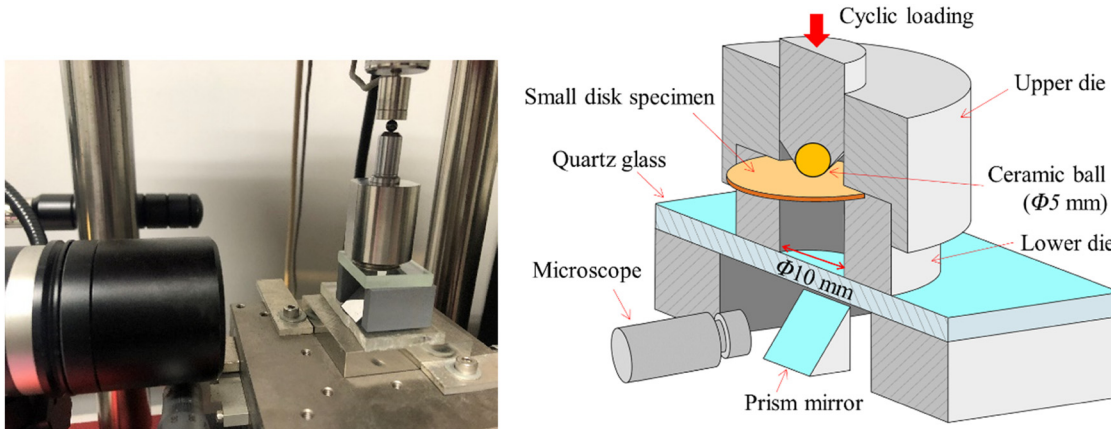**Figure 1:** Microstructure of the tested material.

Figure 2: Photo and schematic illustration of the SPF test.

In this study, the specimen geometries were selected and determined based on the load capacity of the testing machine (max. 100 N). The SiC ball diameter affects the stress distribution in the specimen; the stress distribution gradient increases with the decrease in the ball diameter. Therefore, a ball diameter of 5 mm was determined as the optimum condition for gradual stress distribution. The load ratio of 0.1 was determined because it is impossible to perform under a negative load ratio condition owing to the loading mechanism that involves cyclic ball pushing. Furthermore, the fatigue test results will be almost unaffected by the loading frequency in the tested material at room temperature. Thus, the loading frequency was set as high as possible within the range where self-heating did not occur in the specimen.

The test results are expected to be sensitive to the test conditions, particularly specimen geometry and ball diameter. Further studies regarding the effects of specimen geometry and ball diameter on the test results are essential if SPF tests are conducted under other conditions.

3 Results and discussion

3.1 Morphology of fatigue crack initiation and propagation

Typical fatigue cracks generated on the SD specimen surface during the SPF test are shown in Figure 3. A fatigue crack, which was almost straight, was initiated at the center of the SD specimen (Figure 3(a)). A small fatigue crack was then propagated in the radial direction, and another fatigue crack was generated perpendicular to the original crack (Figure 3(b)). The three fatigue cracks were observed to propagate in the radial direction with point

symmetry toward the center of the SD specimen (Figure 3(c)). Most fatigue cracks propagated in point symmetry and three radial directions (Figure 3), although a few cross-type cracks were observed.

The fatigue crack propagation morphologies could be observed on the surface of the SD specimen because the digital microscope recorded it during the SPF test. The three-dimensional geometry of the fatigue crack on the SD specimen surface could not be observed in the recorded video. In this study, several interrupted specimens with cracks of different lengths were prepared and the three-dimensional geometry of the cracks was measured using X-ray computed tomography (X-CT). A comparison of Figure 4(a) and (d) shows that the crack length measured through X-CT is slightly shorter than that measured by the optical microscope. This is because detecting cracks through X-CT can be challenging if the crack tip mouth is closed, which can result in a shorter crack length measurement compared with an optical microscope.

Figure 5 shows the typical crack shapes measured *via* X-CT, each of which can be approximated by a quarter ellipse. Figure 6 shows the relation between the crack depth c and crack length a measured *via* X-CT. From the results shown in Figure 6 the crack depth, c, can be estimated from the crack length, a, which is measured from the surface of the SD specimen using the following equation:

$$c = 0.2126 + 0.07392 \ln(a). \tag{1}$$

3.2 Evaluation of fatigue strength

3.2.1 Finite element (FE) analysis

Elastic FE analysis was performed using ANSYS[®] Mechanical APDL 2022 R2 to assess the stress distribution in the SD
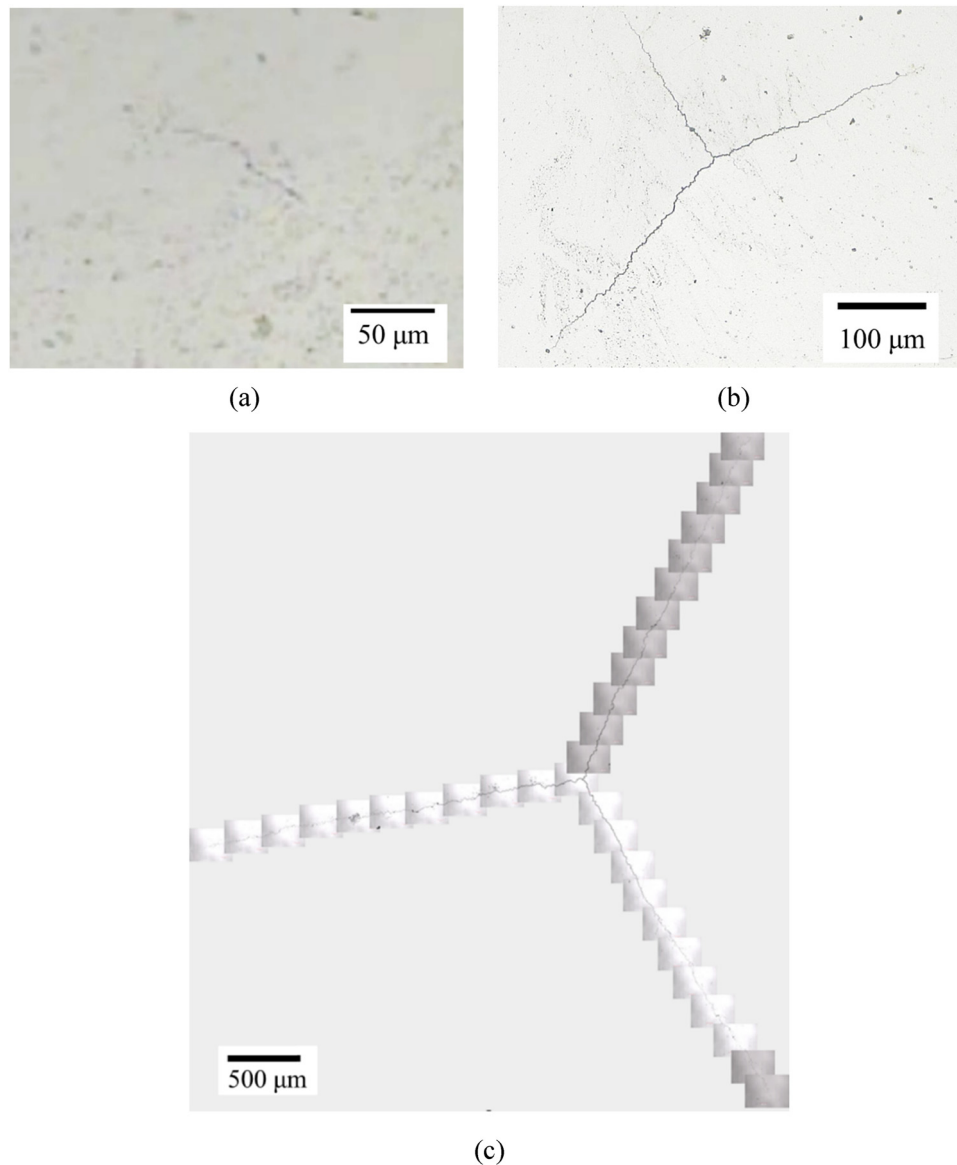
(a)

(b)

(c)

Figure 3: Morphologies of typical fatigue cracks on the SD specimen: (a) just initiated (the still image of the recorded video captured using a digital microscope), (b) after fatigue test, and (c) after crack propagation test.

specimen because the stress field on the SD specimen surface varies with the distance from the center of the specimen in the SPF test. The FE model is illustrated in Figure 7, and the conditions of FE analysis are summarized in Table 3. The two-dimensional model presented in Figure 7, which is axisymmetric and has nodes ranging from 241,188 to 248,891, was used. The stress distribution in the SD specimen was almost independent of the friction coefficients between the SD specimen and SiC ball as well as between the SD specimen and holders; the difference in the stress at the specimen center was less than 1.5% of the maximum circumferential stress. The large deformation in the SD specimen, *i.e.*, large overhang deformation, is speculated to affect the stress distribution. In

addition, the increasing slip between the SD specimen and holder might increase the specimen deformation. Thus, the analysis was performed with zero friction coefficient in this study.

The distributions of the circumferential stress on the bottom surface (tension side) of the SD specimen, obtained through elastic FE analysis, are shown in Figure 8. At the center of the SD specimen, the stress components in the radial and circumferential directions reach their maximum and are the same. However, the circumferential stress is larger than the radial one at any point except for the specimen center, and their difference increases with the increase in the distance from the center of the
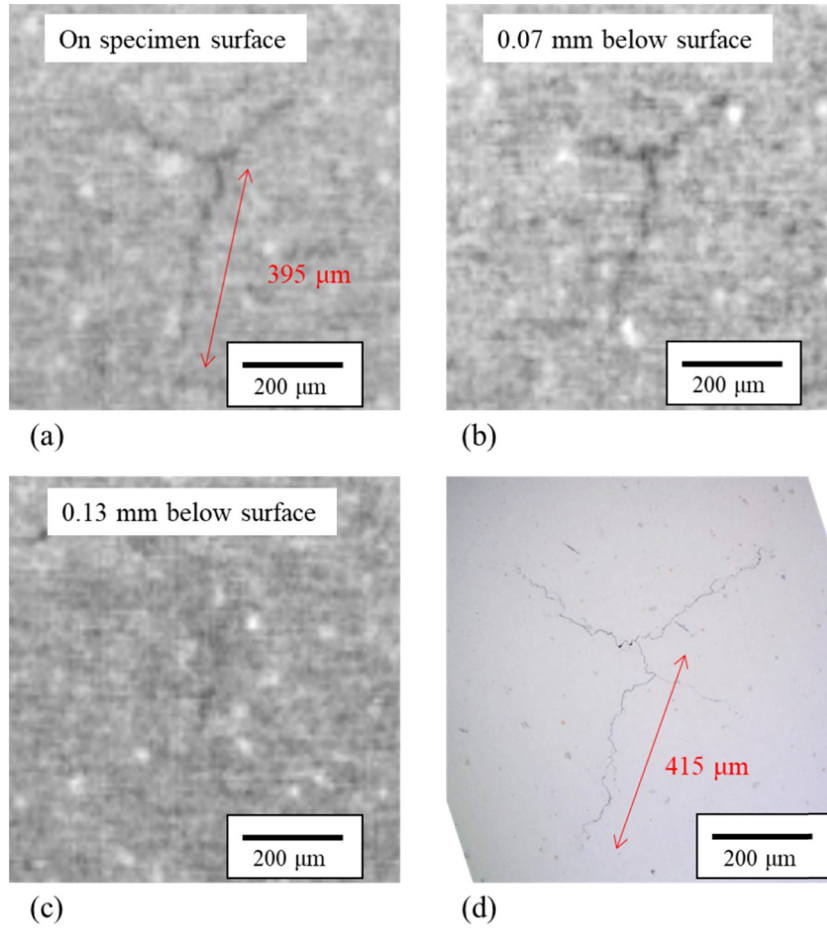
Figure 4: Typical images obtained by X-CT: (a) On the surface of the SD specimen, (b) 0.07 mm below the surface, (c) 0.13 mm below the surface, and (d) optical microscope image.
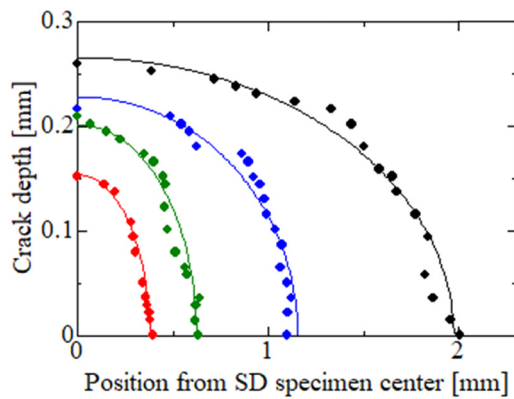

Figure 5: Typical crack shapes measured by X-CT.

Figure 6: Relation between the crack depth and length measured by X-CT.

SD specimen. The results presented in Figure 8 show that a fatigue crack initiates at the center of the SD specimen and propagates in the radial direction.

Figures 9 and 10 demonstrate how the applied load and the thickness of the SD specimen affect the circumferential stress. As shown in Figure 9(a), the circumferential stress at any position increases with the increase in the applied load. However, Figure 9(b) shows that the distributions of the
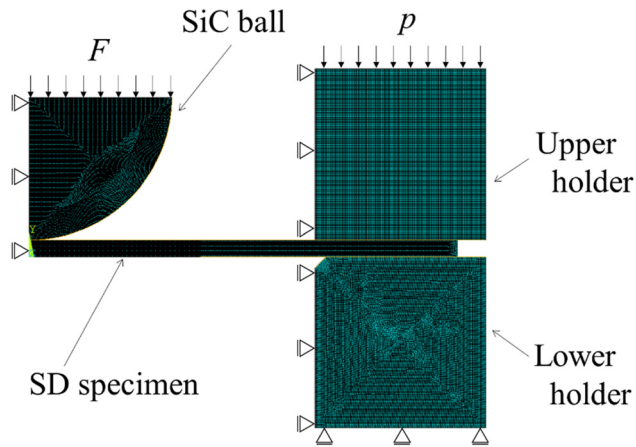
Figure 7: FE model to estimate the stress distribution in the SD specimen.

Table 3: Conditions of FE analysis to evaluate the stress distribution in SD specimen

Young's modulus	SD specimen	204 GPa
	SUS304 holders	193 GPa
	SiC ball	400 GPa
Specimen fix pressure by holders, p		10 MPa
Friction coefficient	SD specimen/ SiC ball	0 and 0.3
	SD specimen/ holders	0 and 0.3
SD specimen thickness		0.285, 0.290, and 0.295 mm
Applied load, F		30, 40, and 50 N
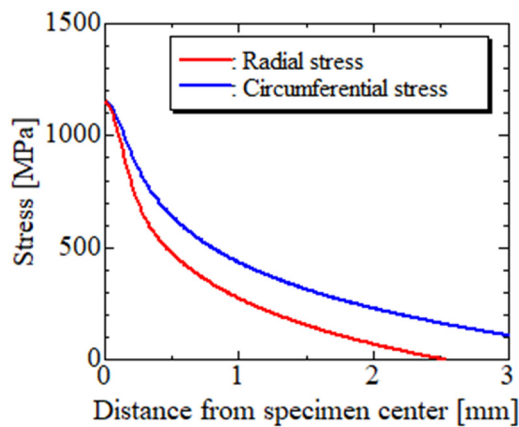
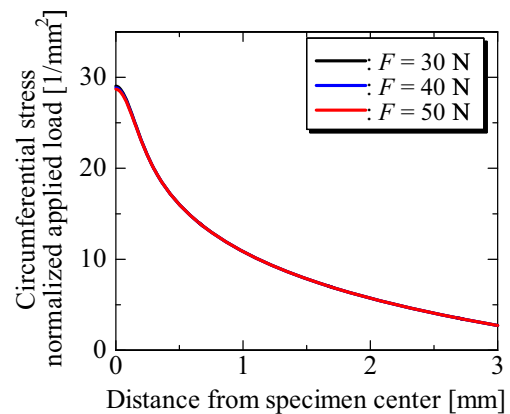**Figure 8:** Typical stress distributions obtained by the FE analysis: applied load, F = 40 N, SD specimen thickness = 0.290 mm.

(a)

(b)

(c)

Figure 9: Effect of the applied load on the circumferential stress: (a) effect on the stress distribution, (b) distribution of circumferential stress normalized by the applied load, and (c) relation between the maximum circumferential stress and the applied load.

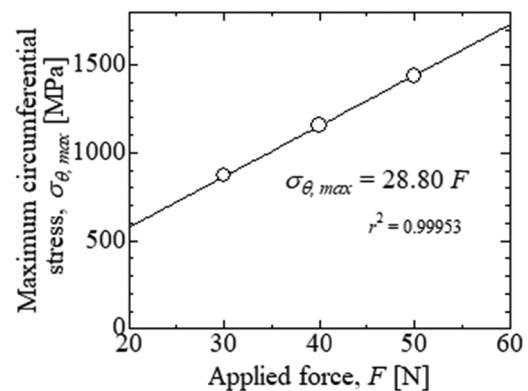circumferential stress normalized by the applied load were independent of the applied load. The maximum circumferential stress $\sigma_{\theta\max}$ is proportional to the applied load (Figure 9(c)). From Figure 9(c), $\sigma_{\theta\max}$ can be evaluated from the applied load F using the following equation:

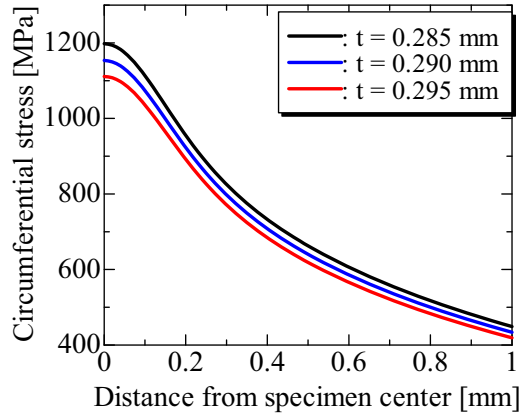$$\sigma_{\theta,\,\max} = 28.80F. \qquad (2)$$

Figure 10: Effect of the SD specimen thickness on the circumferential stress.

As shown in Figure 10, the circumferential stress is affected by the thickness of the SD specimen around its center. However, the difference in stress decreases with the increase in the distance from the center. The thickness of the SD specimen was maintained at 0.290 ± 0.05 in this study. Within the limited thickness, the difference in the maximum circumferential stress due to specimen thickness was negligible as it was less than ±4% (Table 4).

3.2.2 Test results

The results obtained *via* the SPF test are shown in Figure 11. The fatigue data obtained from the CUF test are also included in the figure for comparison. The stress state at the crack initiation point, which is located at the specimen center, is the equibiaxial condition in the SPF test. Thus, the equivalent stress range at the crack initiation point in the SPF test (Figure 11), $\Delta\sigma_{eq}$, is as follows:

$$\Delta\sigma_{eq} = \frac{1}{\sqrt{2}}\sqrt{(\Delta\sigma_r - \Delta\sigma_\theta)^2 + (\Delta\sigma_\theta - \Delta\sigma_z)^2 + (\Delta\sigma_z - \Delta\sigma_r)^2}, \tag{3}$$

Table 4: Effect of specimen thickness on maximum circumferential stress

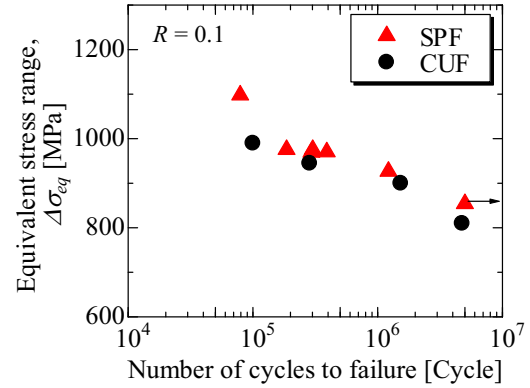| Specimen thickness (mm)	Maximum circumferential stress (MPa)	Difference with data for t = 0.290 mm
0.285	1,198	+3.84%
0.290	1,154	—
0.295	1,111	−3.68%

Figure 11: Fatigue strength obtained from the SPF test.

where $\Delta\sigma_r$, $\Delta\sigma_\theta$, and $\Delta\sigma_z$ represent the stress ranges in the radial, circumferential, and thickness directions of the SD specimen, respectively. Furthermore, $\Delta\sigma_{eq} = \Delta\sigma_\theta$ as $\Delta\sigma_r = \Delta\sigma_\theta$ and $\Delta\sigma_z = 0$ at the center of the SD specimen. As shown in Figure 11, the fatigue lives obtained through the SPF test were nearly equivalent to those obtained *via* the CUF test. This indicates that the SPF test can be used to determine fatigue strength (Figure 11). The IN 718 alloy is a brittle material, and its crystal grain size is sufficiently small compared to the SD specimen thickness. If the SPF test is performed on ductile materials, they might undergo ductile failure instead of fatigue failure owing to ratcheting deformation. Moreover, the crystal orientation of the grain that initiates a fatigue crack may affect the fatigue strength of large-grain materials if the SPF test is applied to large-grain materials. Therefore, verification of the applicability of the SPF test to ductile and large-grain materials is required.

3.3 Evaluation of crack propagation rates

3.3.1 FE analysis of the fracture mechanics parameter

As previously mentioned, most fatigue cracks were found to have propagated in point symmetry and three radial directions, as shown in Figure 3. Thus, to account for this symmetry, a 1/3 model with the crack shown in Figure 12 was used for the FE analysis to estimate the stress intensity factor (SIF). Three-dimensional (3D) FE analysis was performed using ANSYS® Workbench 2022 R2. The total number of nodes in the model used for the 3D FE analysis were 118,840–431,125. As shown in Figure 12, the FE model, each cross-section of the SD specimen, the holders, and the SiC ball are set as the periodic symmetric boundary. This study assumed a quarter ellipse shape for the fatigue crack based on the results of X-CT, as shown in Table 5.
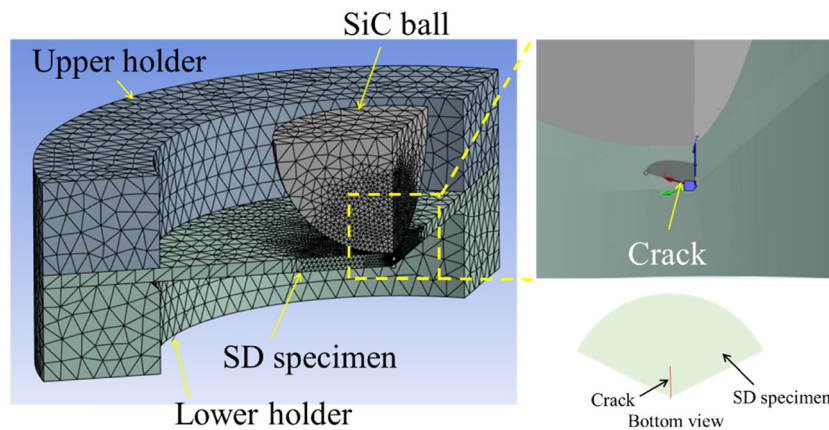
Figure 12: FE model to evaluate the SIF.

Table 5: Conditions of FE analysis to evaluate the SIF

Young's modulus (GPa)	SD specimen	204
	SUS304 holders	193
	SiC ball	400
Specimen fix pressure by holders, p (MPa)		10
Friction coefficient	SD specimen/SiC ball	0
	SD specimen/holders	0
SD specimen thickness (mm)		0.290
Applied load, F (N)		30, 40, and 50
Crack size, (a, c) (mm)		(0.3, 0.1236), (0.5, 0.1614), (0.75, 0.1914), (1.0, 0.2126), and (1.5, 0.2638)

The impact of the applied load on the SIF obtained through FE analysis is illustrated in Figure 13. The SIF distributions along the crack leading edge, as shown in Figure 14, are represented in Figure 13; the average node spacing along the crack leading edge was approximately 2 μm. As shown in Figure 13(a), the SIF increases with the increase in the applied load. However, Figure 13(b) reveals that the SIF distributions normalized by the applied load were independent of the applied load, similar to the stress distribution shown in Figure 9.

Figure 15 illustrates the impact of the crack geometry on the SIF. When the crack length is relatively short (almost less than 0.5 mm), the SIF is almost uniform along the crack leading edge. However, as the crack length

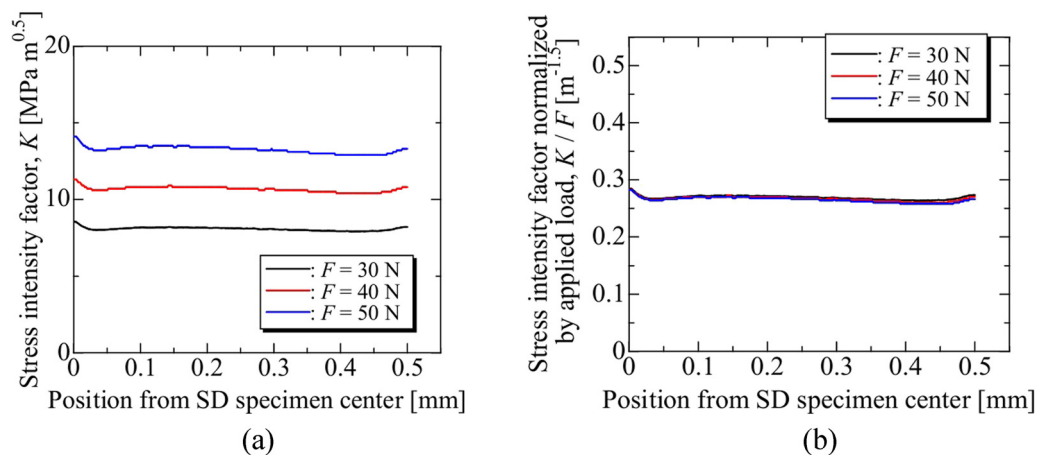**Figure 13:** Effect of the applied load on the SIF: (a) Distribution of SIF, (b) Distribution of SIF normalized by applied load.
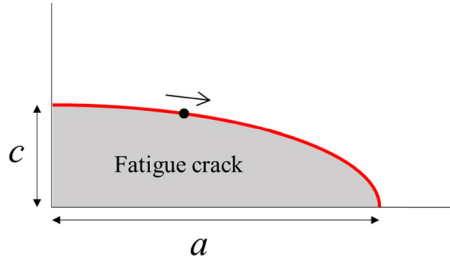
Figure 14: Schematic illustration of the definition of the position for calculating the SIF along the crack leading edge.
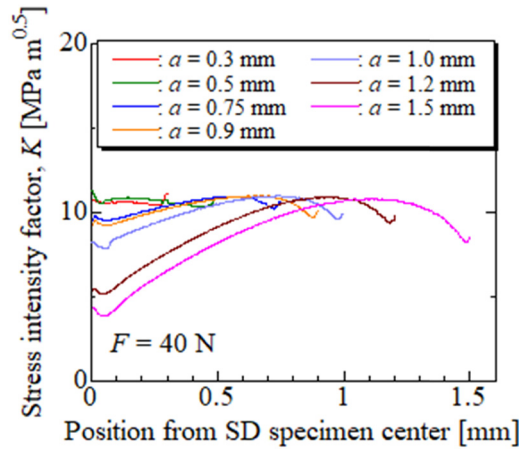

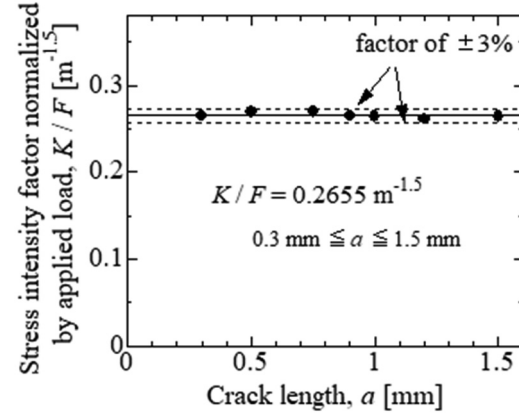**Figure 15:** Effect of the crack geometry on the SIF.

Figure 16: Relation between the SIF obtained from the FE analysis and the crack length.

$$K = \sigma \sqrt{\pi a}\, B, \qquad (4)$$

where B represents the shape coefficient. In the conventional fatigue crack propagation test on a compact tension (CT) specimen or center-notch specimen under constant-load conditions, the SIF increases with crack growth. However, the results presented in Figure 15 indicate that the SPF test enables the fatigue crack propagation tests under a constant SIF condition. In the SPF test, the SIF remains unaffected by changes in the crack length because the stress at the crack tip decreases with the increase in the crack length.

Based on the aforementioned results, this study evaluated the crack growth rate in the crack length range of 0.3–1.5 mm. The SIF range ΔK was calculated using the following equation:

$$\Delta K = 0.2655(F_{max} - F_{min}) = 0.2655\,(1 \\ - R)F_{max}\ (0.3\ \text{mm}\ \leq a \leq 1.5\ \text{mm}), \qquad (5)$$
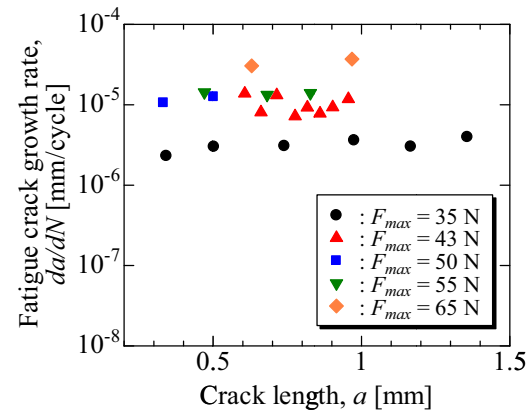
increases, the distribution of the SIF becomes nonuniform. When the crack length exceeds 1 mm, the SIF around the center of the SD specimen decreases considerably. This decrease in SIF around the center of the SD specimen with the increase in the crack length is related to the crack geometry. A comparison of Figures 5 and 15 shows that the area with a low SIF corresponds to the area where the crack tip extends beyond the neutral plane of the specimen. Based on the results presented in Figures 5 and 15, it can be concluded that the fatigue crack is unlikely to penetrate through the thickness of the specimen as the driving force for crack growth is reduced around the center of the SD specimen.

Based on the results obtained and the crack length measured at the SD specimen surface, the SIF for the given crack length was determined. The SIF was calculated as the average value along the crack leading edge in the region from the SD crack surface to a depth of 50% of the surface (*i.e.*, to the neutral plane). Figure 16 shows the relation between the SIF and crack length. The SIF remains constant and independent of the crack length. Generally, the SIF, K, is represented by the crack length a and applied stress σ as follows:

Figure 17: Relation between the fatigue crack growth rate, d*a*/d*N*, and the crack length, *a*.

where F_{max} and F_{min} represent the maximum and minimum applied forces in the SPF test, respectively, and R represents the load ratio (F_{min}/F_{max}).

3.3.2 Test results

The SPF test was performed to investigate the behavior of crack growth. a is defined as the average distance between the specimen center and crack tip for three radial cracks.

Figure 17 shows the relation between the fatigue crack growth rate (da/dN) and a obtained *via* the SPF test. This relation indicates that the crack growth rate increased with the increase in the applied load. The findings shown in Figure 17 reveal that the crack propagation tests under the constant SIF condition can be conducted *via* the SPF test, as the crack growth rates are almost independent of the crack length at the given load condition.

Figure 18 shows the crack growth rate correlated with the SIF range obtained from the average crack length using equation (5). For comparison, the crack growth curves reported in previous studies are also shown in Figure 18 [19,20]. As observed in Figure 18, the crack growth rates obtained *via* the SPF test are relatively higher than those reported in the previous studies. However, the difference in the crack propagation test results between this study and the previous studies is not significant.

The reference data shown in Figure 14 are obtained for relatively large crack sizes using single-edge notched bend specimens or compact-tension specimens. Furthermore, the crack growth data in this study were evaluated for the surface cracks whose lengths were less than 1.5 mm.
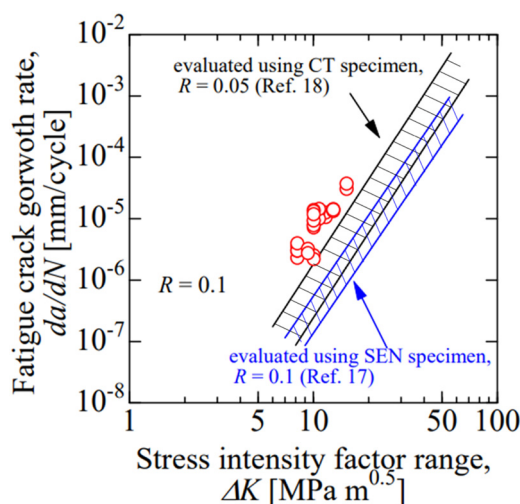
The difference in the crack propagation rates shown in Figure 14 might be related to the crack size difference, *i.e.*, the "small crack effect" [21].

The aforementioned results indicate that the SPF test can be used to conduct a constant-SIF range test. However, further verification is required to determine the applicability of the SPF test to ductile and large-grain materials for crack propagation testing.

4 Conclusion

Herein, the morphologies of fatigue crack initiation and propagation for the Ni-based superalloy IN 718 were investigated through the SPF test to verify the applicability of this test in evaluating fatigue lives and crack growth rates.

The main conclusions can be summarized as follows.

(1) A fatigue crack was found to initiate at the center of the SD specimen surface, where stress was the maximum. In most cases, three fatigue cracks propagated from the center to the radial direction of the SD specimen in point symmetry.

(2) X-CT results revealed that the fatigue crack initiated by the SPF test had a quarter ellipse shape. Based on these results, an approximate equation was obtained to calculate the crack depth from the measured crack length for the SD specimen.

(3) When the fatigue lives evaluated *via* the SPF test were related to the range of the maximum stress at the SD specimen center obtained through elastic FE analysis, the fatigue strength determined *via* the SPF test was almost comparable with that determined *via* the CUF test.

(4) The elastic FE analysis results indicated that the SIF for the fatigue crack in the SD specimen was independent of the crack length; further, it could be calculated *via* the approximate equation using the applied load regardless of the crack length.

(5) The results of the crack propagation test and elastic FE analysis confirm that the SIF test can be used to conduct a constant-SIF crack propagation test.

Based on the aforementioned results, the applicability of the SPF test to assess fatigue strength and crack propagation behavior was confirmed.

Figure 18: Fatigue crack propagation rates obtained by the SPF test correlated with the SIF range.

Author contributions: Yasuhiro Yamazaki: conceptualization, methodology, data curation, writing – original draft,

References

[1] Zhu M, Liu X, Lai J, Luo J. Fatigue life of a pressure vessel based on residual strength and crack size. Trans Can Soc Mech Eng. 2022;46:391–9.

[2] Gao J, Heng F, Yuan Y, Liu Y. A novel machine learning method for multiaxial fatigue life prediction: improved adaptive neuro-fuzzy inference system. Int J Fatigue. 2024;178:108007.

[3] Thombre SC, Kotwal MR. Residual life assessment. Int J Eng Res Technol. 2015;4:1068–75.

[4] Kadoya Y, Goto T, Date S, Yamauchi T, Saida T, Sada T. Assessment of remaining life of fossil power plant parts by means of a miniature creep rupture test. ISIJ Int. 1990;30:854–61.

[5] Liaw PK, Saxena A, Schaefer J. Estimating remaining life of elevated-temperature steam pipes – part I. Materials properties. Eng Fract Mech. 1989;32:675–708.

[6] Garzillo A, Guardamagna C, Moscotti L, Ranzani L. A technique for the residual life assessment of high temperature components based on creep-rupture testing on welded miniature specimens. Int J Pressure Vessels Piping. 1996;66:223–32.

[7] Liaw PK, Rao GV, Burke MG. Creep fracture behavior of 214Cr 1Mo welds from a 31-year-old fossil power plant. Mater Sci Eng A. 1991;131:187–201.

[8] Oka M, Yakushiji T, Tsuchida Y, Enokizono M. Nondestructive evaluation of fatigue damage in the stainless steel by using electromagnetic method. E-J Adv Maint. 2009;1:77–82.

[9] Sposito G, Ward C, Cawley P, Nagy PB, Scruby C. A review of non-destructive techniques for the detection of creep damage in power plant steels. NDT&E Int. 2010;43:555–67.

[10] Dzugan J, Konopík P. Small punch test application to material properties evolution determination. J Solid Mech Mater Eng. 2012;6:782–91.

[11] Suzuki M, Eto M, Fukaya K, Nishiyama Y, Kodaira T, Oku T. Estimation of toughness degradation by microhardness and small punch tests. Small specimen test techniques. ASTM STP. 1993;1204:217–27.

[12] Bruchhausen M, Holmström S, Simonovski I, Austin T, Lapetite J-M, Ripplinger S, et al. Recent developments in small punch testing: tensile properties and DBTT. Theor Appl Fract Mech. 2016;86:2–10.

[13] Ule B, Šuštar T, Dobeš F, Milička K, Bicego V, Tettamanti S, et al. Small punch test method assessment for the determination of the residual creep life of service exposed components: outcomes from an interlaboratory exercise. Nucl Eng Des. 1999;192:1–11.

[14] Holmström S, Li Y, Dymacek P, Vacchieri E, Jeffs SP, Lancaster RJ, et al. Creep strength and minimum strain rate estimation from small punch creep tests. Mater Sci Eng A. 2018;731:161–72.

[15] Ortiz-Mariscal A, Saucedo-Muñoz ML, Naveena KS, Komazaki S. Application of small punch creep testing for evaluation of creep properties of as-received and artificially aged 5Cr-0.5Mo steel. Mater Sci Eng A. 2018;709:322–9.

[16] Komazaki S, Sugimoto T, Hasegawa Y, Kohno Y. Damage evaluation of a welded joint in a long-term service-exposed boiler by using a small punch creep test. ISIJ Int. 2007;47:1228–33.

[17] Lancaster RJ, Jeffs SP, Illsley HW, Argyrakis C, Hurst RC, Baxter GJ. Development of a novel methodology to study fatigue properties using the small punch test. Mater Sci Eng A. 2019;748:21–9.

[18] Yamazaki Y, Sugaya R, Kobayashi U, Ohta Y. Effects of thermal cycling and microstructure on the fatigue crack propagation in forged titanium–aluminide alloys under thermomechanical fatigue conditions. Mater Sci Eng A. 2020;797:140248.

[19] Mercer C, Soboyejo ABO, Soboyejo WO. Micromechanisms of fatigue crack growth in a forged inconel 718 nickel-based super-alloy. Mater Sci Eng A. 1999;270:308–22.

[20] James LA. Fatigue crack propagation in alloy 718: a review. Superalloys. 1989;499–515.

[21] Phillips EP, Newman JC. Impact of small-crack effects on design life calculations. Exp Mech. 1989;29:221–5.